Available online at www.sciencedirect.com
ScienceDirect
Journal of Catalysis 252 (2007) 249–257
JOURNAL OF CATALYSIS
www.elsevier.com/locate/jcat

Defect-induced strategies for the creation of highly active hydrotalcites in base-catalyzed reactions

R.J. Chimentão [a], S. Abelló [a], F. Medina [a,*], J. Llorca [b], J.E. Sueiras [a], Y. Cesteros [c], P. Salagre [c]

[a] *Dept. d'Enginyeria Química, Universitat Rovira i Virgili, 43007 Tarragona, Spain*
[b] *Institut de Tècniques Energètiques, Universitat Politècnica de Catalunya, Diagonal 647, 08028 Barcelona, Spain*
[c] *Dept. de Química Inorgánica, Universitat Rovira i Virgili, 43007 Tarragona, Spain*

Received 1 June 2007; revised 25 July 2007; accepted 25 September 2007

Available online 26 October 2007

Abstract

Mg–Al hydrotalcites have demonstrated their superior performance in numerous base-catalyzed applications, especially their meixnerite-type analogues. The effect of using mechanical stirring or ultrasound during reconstruction of the mixed oxides leads to an enhancement in the catalytic activity. This can be correlated to modifications in the structure and basicity of the resulting materials, together with an increased surface area and improved accessibility to the active sites. However, increasing the rehydration time during stirring or sonication strongly affects the final catalyst, as observed by high-resolution transmission electron microscopy. An important amount of defects in the lamellar structure of the small hydrotalcite nanoplatelets are likely responsible of the presence of stronger and more accessible active basic sites, as determined by CO_2-TPD and benzoic acid titration. The greater performance of these materials has been disclosed for the epoxidation of styrene.

Keywords: Hydrotalcite; Rehydration; Exfoliation; Nanoplatelets; Ultrasounds; Styrene epoxidation

1. Introduction

The increasing environmental pressure on industry to replace traditional homogeneous catalysts by friendly technologies represents one of the most relevant driving forces for the development of new heterogeneous catalysts. However, understanding the performance of basic sites in these heterogeneous systems requires the systematic design of strategies that evidence clear structure–activity relationships at an atomic level. This is the case for activated hydrotalcites, which have been widely studied in recent years in the search for strategies for resolving their unparalleled activity, particularly their reconstructed mixed oxides. Hydrotalcites are layered double hydroxides with the general formula $[M^{2+}_{1-x}M^{3+}_{x}(OH)_2][X^{m-}]_{x/m}\cdot nH_2O$, consisting of brucite-type octahedral layers, in which M^{2+} cations are partially substituted by M^{3+} cations. The net positive charge resulting from this substitution is compensated for by anions (typically carbonate), located together with water molecules in the interlayer space [1]. These materials are often inactive and must be activated by thermal decomposition to obtain a high-surface area and well-dispersed Mg(Al)O mixed oxide. In the presence of water and appropriate anions, the oxide mixture can be reconstructed back to the original hydrotalcite structure. This property, known as memory effect, provides an effective synthetic pathway for the insertion of organic and inorganic anions into the hydrotalcite. A particular example of this is meixnerite, which contains OH^- groups in the interlayer space after the mixed oxide is contacted with decarbonated water or in a flow of gas saturated with water [2,3]. This material exhibits outstanding activity for base-catalyzed reactions, requiring the presence of Brønsted sites [4–6]. However, many applications are largely restricted, due to inaccessibility to the inner surfaces of the OH^- hosted layers [7]. The original hypothesis of Roelofs et al. [8] claimed that the active sites are likely situated at the edges of nanoplatelets, which represent a minor part of the Brønsted sites in the hydrotalcite. So far, this in-

* Corresponding author.
E-mail address: francesc.medina@urv.cat (F. Medina).

0021-9517/$ – see front matter
doi:10.1016/j.jcat.2007.09.015

formation has been obtained indirectly, by correlating ex situ characterization of the catalysts with specific trends in catalytic performance. Consequently, several studies have been conducted to maximize the number of edge sites, hereby inducing a more irregular platelet morphology [9,10]. This was achieved by preparating small hydrotalcite nanoplatelets (≈20 nm) supported on carbon nanofibers [11] or by using ultrasound for short periods during reconstruction [9], leading to impressive enhancement of the catalytic activity in the aldol condensation reaction of citral and acetone. This was previously attributed to the increased surface area of the resulting meixnerite, thus leading to an increased number of exposed OH^- sites. Very recently, Roeffaers et al. [12] were able to map the spatial distribution of catalytic activity over an entire hydrotalcite crystal by means of wide-field fluorescence microscopy. They demonstrated the existence of basic sites of different strength when comparing crystal faces, defects, or edges, the latter containing the stronger basic sites. Accordingly, the most effective solution to maximize the utility of the platelets (i.e., the edges of the hydrotalcites) involves their break up into thinner layers.

In this paper, the use of ultrasound or high mechanical stirring for longer times during rehydration has been attempted to deliberately produce irregularities in the agglomeration of layers. With long sonication treatment, surface areas remain practically constant, but the distortions on the crystalline structure, as determined by HRTEM, leads to important differences in terms of catalytic activity. The latter can be associated with the existence of stronger basic sites at the defects produced by sonication. The catalytic role of the basic sites has been envisaged through the base-catalyzed epoxidation of styrene, whereas determination of their inherent basicity has been assessed by poisoning with benzoic acid. A linear correlation between reaction rates and number of active sites has been found for the rehydrated hydrotalcites by mechanical stirring, whereas 2 intersecting linear segments were observed for the sonicated materials, thus confirming the presence of different types of basic sites.

2. Experimental

2.1. Materials and methods

The Mg–Al hydrotalcite (Mg/Al molar ratio = 4) was prepared by coprecipitation at constant pH of an aqueous solution of $Mg(NO_3)_2{\cdot}6H_2O$ (1 M) and $Al(NO_3)_3{\cdot}9H_2O$ (1 M) and a second solution of NaOH (2 M). Both solutions were mixed dropwise under stirring at 298 K and inert atmosphere, and after the reactants were added, the slurry was aged for 18 h at room temperature. The resultant slurry was filtered and thoroughly washed with deionized water and finally dried at 383 K to yield the as-synthesized hydrotalcite (HT-asy). This sample was calcined at 723 K in air for 48 h to obtain the corresponding Mg(Al)O mixed oxide (HT-cc). This material was reconstructed in decarbonated water (0.05 g in 5 ml of water) under high mechanical stirring (500 rpm) for different times (25 min, 4 h, and 24 h) or by sonication (25 and 50 min). The reconstructed samples, denoted hereafter as HT-rm(25 min), HT-rm(4 h) and HT-rm(24 h), or HT-rus(25 min) and HT-rus(50 min) (according to the reconstruction by mechanical stirring or by ultrasonication, respectively), were kept under inert atmosphere for further use.

The chemical composition of the samples was determined by ICP-OES with a Perkin-Elmer Plasma 400 instrument. X-ray diffraction (XRD) measurements were made using a Siemens D5000 diffractometer (Bragg-Bentano parafocusing geometry and vertical θ–θ goniometer) fitted with a grazing incident (ω: 0.52°) attachment for thin film analysis and scintillation counter as a detector. The samples were dispersed on Si (510) sample holder. The angular 2θ diffraction range was between 5° and 70°. The data were collected with an angular step of 0.03° at 12 s per step and sample rotation. CuK_α radiation (λ = 1.54056 Å) was obtained from a copper X-ray tube operated at 40 kV and 30 mA. The crystalline phases were identified using the JCPDS files. High-resolution transmission electron microscopy (HRTEM) studies were conducted using a JEOL JEM 2010F electron microscope equipped with a field emission gun, working at an accelerating voltage of 200 kV. Samples were dispersed in ethanol in an ultrasonic bath, and a drop of supernatant suspension was poured onto a holey carbon coated grid and dried completely before measurements. N_2 adsorption and desorption isotherms at 77 K were measured on a Micromeritics ASAP 2000 surface analyzer. Before analysis, the samples were degassed under vacuum at 393 K for 16 h. Thermal analysis was performed in a Perkin-Elmer TGA 7 thermobalance equipped with a programmable temperature furnace. The sample (50 mg) was heated from room temperature up to 1073 K in argon (80 ml min^{-1}) at 5 K min^{-1}. Temperature-programmed desorption (TPD) of CO_2 of rehydrated samples was studied using a TPD/R/O 1100 (Thermo-Finnigan) equipped with a TCD detector and coupled to a mass spectrometer (Omnistar QMS 422). Before TPD, the samples (200 mg) were treated at 353 K with 3% CO_2/He flow (20 ml min^{-1}) for 1 h. After that, desorption was carried out from 353 to 1173 K at 10 K min^{-1} in He flow. Determination of the base amount of the catalysts was also estimated by titration using benzoic acid.

2.2. Catalytic measurements

The epoxidation of styrene was performed in a batch reactor at 313 K and atmospheric pressure. Typically, styrene (4 mmol), acetone 8.0 ml (0.136 mol), acetonitrile 6.3 ml (0.153 mol), water (5 ml), H_2O_2 (3 ml at 33% in water), and 50 mg of catalyst (calcined or rehydrated hydrotalcite) were introduced in the reactor. In addition, catalytic activity tests without the addition of water in the reaction medium were performed. H_2O_2 efficiency was determined by $KMnO_4$ titration. Samples were obtained at regular periods and analyzed offline by a Shimadzu GC-17 gas chromatograph with an Ultra 2 capillary column (15 m × 0.32 mm × 0.25 μm) a flame ionization detector. All of the reactants were purchased from Aldrich and used without further purification.

3. Results and discussion

3.1. X-ray diffraction

The layered structure of the as-synthesized and rehydrated hydrotalcites was confirmed by XRD, as shown in Fig. 1. The XRD pattern of the as-synthesized (HT-asy) sample exhibited sharp and symmetric reflections for the (003), (006), and (009) planes and broad symmetric peaks for the (110) and (113) planes, which are characteristic of hydrotalcite-like materials (JCPDS 22-700). The reflections correspond to a hexagonal lattice with $R3m$ rhombohedral symmetry. The (003) and (006) reflections, at 11.6° and 23.4°, respectively, were used to calculate the basal spacing between the layers, d. The (110) reflection was used to calculate the unit cell dimension, a, where $a = 2d_{110}$ [13]. The results of these calculations are shown in Table 1. The lack of the (00l) reflections in the XRD pattern of the calcined product at 723 K (HT-cc sample in Fig. 1f) indicates that the layered structure of the HT has been destroyed by calcination. For the HT-cc, the characteristic reflections observed at $2\theta \approx 43$ and 63° correspond to a Mg–Al–O (periclase-like structure, JCPDS 87-0653). This observation was also confirmed by HRTEM.

Reconstruction of the calcined samples resulted in the recovery of the layered structure back to meixnerite (JCPDS 35-0965), as a result of the well-known "memory effect" [14], in which the presence of water restores the interlayer hydrogen bonding network and gallery spacing while the original nitrate anions in the as-synthesized hydrotalcite have been replaced by Brønsted OH sites [15–17]. The X-ray patterns of the rehydrated samples are depicted in Fig. 1, b–e. One of the most striking features for the platelet-like sample is the loss of intensity of sharp basal peaks, particularly for the sonicated samples [HT-rus(25 min) and HT-rus(50 min)], which appear as broad reflections. This could indicate that the sonication treatment leads to a more amorphous structure with smaller crystals, in which the agglomeration of platelets is more exfoliated. Exfoliation is consequently considered as the reduction of the stacking of layers. The (110) reflection is discerned at 60.5°, indicating that the two-dimensional crystalline order of LDH was still preserved. The new term *nanosheets* [18] has been widely accepted to represent this two-dimensional anisotropy (typically of micrometer lateral size and nanometer thickness), of the individual host layers. It is noteworthy that similar broad profiles have been taken as providing evidence of disordered layered materials [19].

Table 1
Surface area and lattice parameters of the hydrotalcite samples

Sample code	Mg:Al atom ratio[a]	Surface area ($m^2\ g^{-1}$)	d_{003} (Å)	d_{110} (Å)	a (Å)
HT-asy	3.90	25	8.016	1.522	3.044
HT-cc	3.90	196	–	–	–
HT-rm(25 min)	3.88	215	8.113	1.516	3.032
HT-rm(4 h)	3.91	286	8.045	1.512	3.024
HT-rus(25 min)	3.90	437	8.135	1.511	3.022
HT-rus(50 min)	3.87	466	8.106	1.514	3.028

[a] ICP-OES.

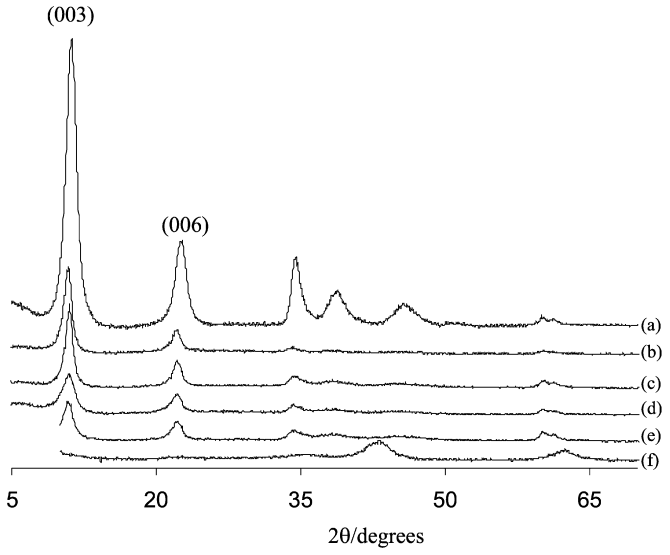

Fig. 1. X-ray diffraction of the LDHs materials. (a) HT-asy; (b) HT-rm(25 min); (c) HT-rm(4 h); (d) HT-rus(25 min); (e) HT-rus(50 min); and (f) HT-cc.

3.2. HRTEM

To investigate the morphology and microstructure at an atomic level of the hydrotalcite samples obtained after rehydration under mechanical stirring or ultrasound, as well as of the calcined sample, an accurate HRTEM study was performed. Low-resolution TEM images of these materials are shown in Fig. 2. In all cases, a platelet morphology characteristic of hydrotalcite-type materials was observed. However, platelets in the sample obtained after rehydration under mechanical stirring (Fig. 2b) are generally larger than those seen in the sample obtained by rehydration under ultrasound (Fig. 2c), which in turn are similar to those present in the calcined sample (Fig. 2a). Although no noticeable change in the morphology of the samples was detected at low magnification, important differences were observed in the lattice fringe images obtained at higher magnification under HRTEM conditions. Fig. 3 corresponds to a HRTEM image of the calcined sample. The inset corresponds to the Fourier transform (FT) image of the crystallographically oriented crystallite in the center of the HRTEM image. Spots at 2.4 and 2.1 Å correspond to the (111) and (200) planes, respectively, of the periclase structure. The relative position of the spots in the FT image indicate that the crystallite is oriented along the (011)-type crystallographic direction. Selected-area electron diffraction patterns (SAED) recorded over several areas show that the calcined sample comprises mainly the periclase structure (rings at 2.4, 2.1, and 1.5 Å), although minor amounts of the original hydrotalcite phase are still recognizable (at 3.8 and 2.6 Å).

Fig. 4 corresponds to a representative HRTEM picture of the sample rehydrated under mechanical stirring [HT-rm (24 h)]. The sample is constituted by crystallites showing well-developed platelet morphology. The platelet at the center of the image in Fig. 4 is crystallographically oriented, and a portion of its lattice-fringe image (inside the marked square) is enlarged

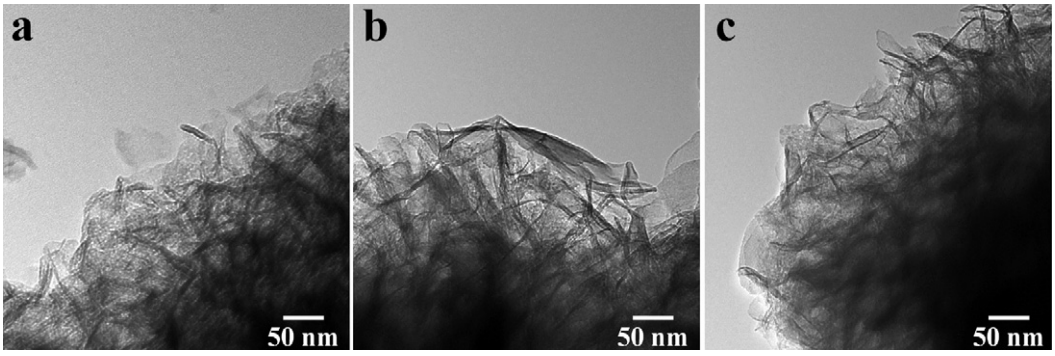

Fig. 2. Low-magnification, bright-field transmission electron microscopy images of the calcined sample (a), and rehydrated samples obtained under mechanical stirring (b) and ultrasounds (c) treatments.

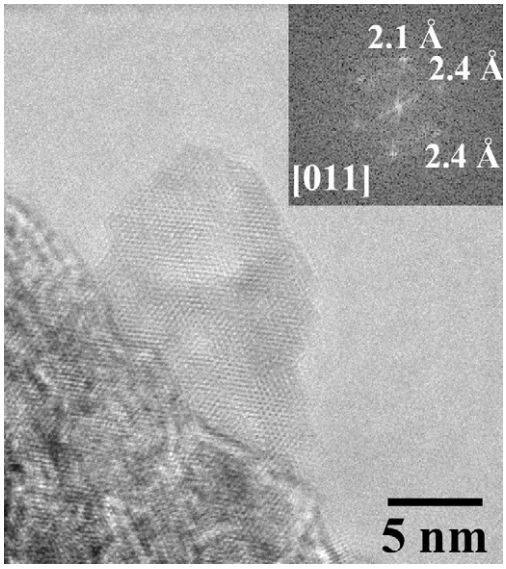

Fig. 3. HRTEM image corresponding to the calcined sample and FT image of the oriented crystallite at the center of the image.

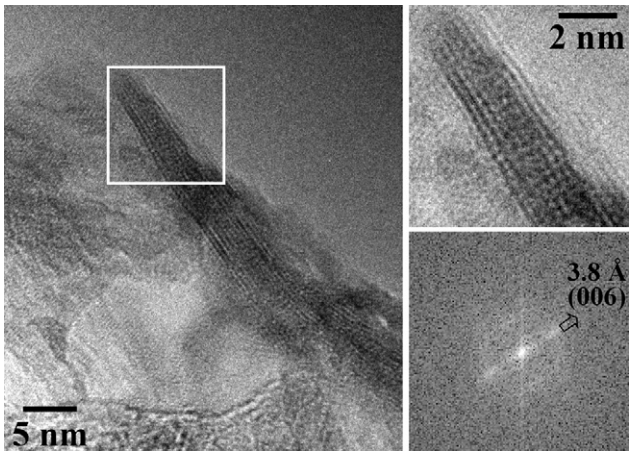

Fig. 4. HRTEM image corresponding to the rehydrated sample under mechanical stirring (HT-rm(24 h)). The inset shows the enlargement of the area enclosed by the square and its corresponding FT image.

and showed apart, along with the corresponding FT image. Spots at 3.8 Å correspond to (006) planes of the hydrotalcite phase, thus indicating that the platelet is oriented perpendicular

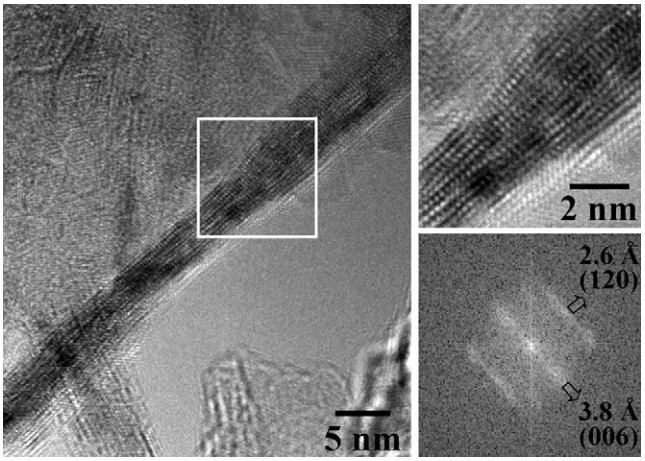

Fig. 5. HRTEM image corresponding to the rehydrated sample under ultrasounds (HT-rus(50 min)). The inset shows an enlarged view of the area enclosed by the square and its corresponding FT image.

to the *c* crystallographic axis, or, in other words, that the basal plane of the platelets coincides with the *ab* crystallographic plane of the hydrotalcite structure. The enlarged image has atomic resolution and shows a generally well-ordered array of atomic rows with little structural distortion. Fig. 5 corresponds to a similar analysis performed over the sample rehydrated under ultrasounds [HT-rus(50 min)], which displays important differences with respect to the sample rehydrated under mechanical stirring.

The FT image corresponding to the enlarged area of the platelet enclosed in the square in Fig. 5 does not show single spots at 3.8 Å corresponding to (006) planes of the hydrotalcite phase, as were seen in the sample rehydrated under mechanical stirring (Fig. 4). Instead of this, in the FT image of the sample rehydrated under ultrasounds there are parallel strings of spots that are indicative of short-range atomic ordering. Within the main string, spots around 3.8 Å are brighter, corresponding to (006) planes, whereas the strings are separated at exactly 2.6 Å, corresponding to (120) planes in the basal plane of the platelet. The lack of single spots and the presence of the strings in the FT image are interpreted in terms of a highly disordered structure for the hydrotalcite phase obtained by rehydration under ultrasounds. This can be clearly seen at the atomic scale in the enlarged, direct-space HRTEM inset of Fig. 5, in which

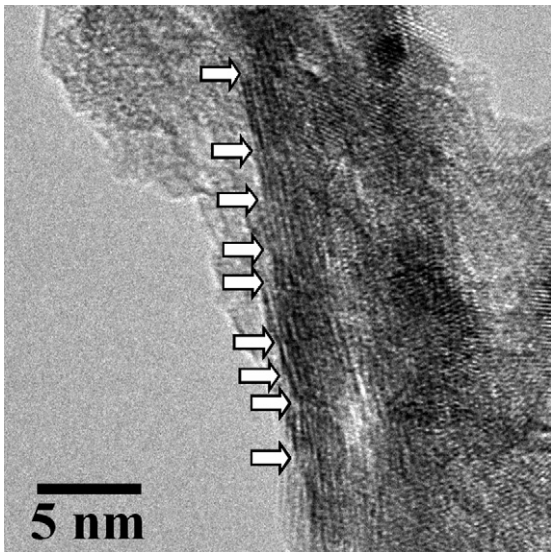

Fig. 6. HRTEM image corresponding to the rehydrated sample under ultrasounds (HT-rus(50 min)). Several structural defects are marked by arrows.

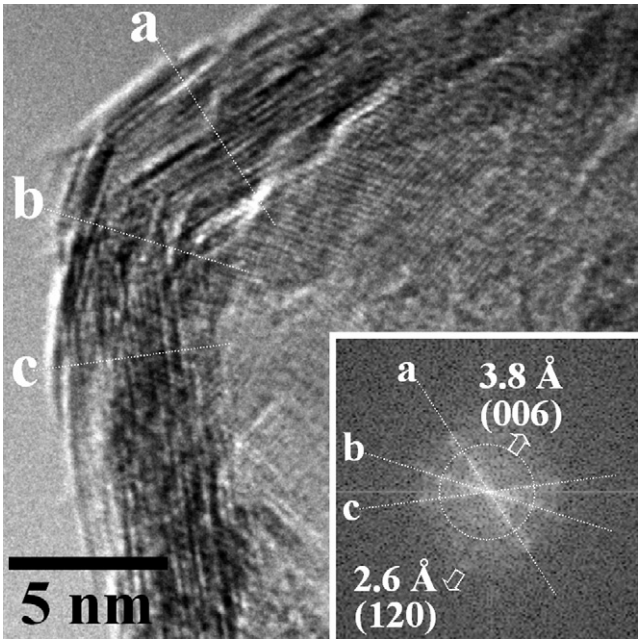

Fig. 7. HRTEM image corresponding to the rehydrated sample under ultrasounds, HT-rus(50 min), and its associated FT image.

high-density of structural defects can be readily identified. The hydrotalcite platelets maintain the same crystallographic habit as in the sample rehydrated under mechanical stirring (i.e., with the basal plane perpendicular to the *c* crystallographic axis), but in the sample rehydrated under ultrasounds, the extent of well-ordered arrays of atomic rows within the hydrotalcite platelets is limited due to the existence of numerous irregularities in the crystals. The linear defects produced by sonications are also depicted in Fig. 6, with the main irregularities clearly indicated by arrows.

Another representative HRTEM image of the rehydrated sample under ultrasound is shown in Fig. 7. In this case, several platelets are stacked and curved together. The FT image (Fig. 7, inset) shows three different strings of spots that correspond to the different orientation of platelets following three different directions (labeled "*a*," "*b*," and "*c*"). Within the strings, spots due to (006) planes of the hydrotalcite structure at 3.8 Å are recognizable, but again, the presence of the strings is indicative for the existence of distortions in the platelets. Spots at 2.6 Å correspond to (120) planes of the hydrotalcite structure and are located in the FT image perpendicular to the string labeled as "*b*," thus indicating that they belong to the basal plane of platelets "*b*." SAED patterns recorded for rehydrated samples both under mechanical stirring and ultrasounds exhibit rings corresponding to the hydrotalcite phase, but also some minor amount of the periclase structure, which constitutes the bulk of the calcined sample. This indicates that the rehydration of the periclase structure into meixnerite is almost complete in both cases.

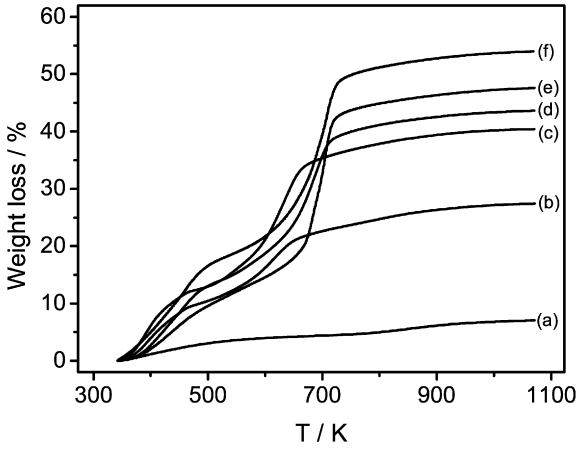

Fig. 8. Thermogravimetric analysis of the hydrotalcite samples. (a) HT-cc; (b) HT-rm(25 min), (c) HT-rm(4 h) and (d) HT-rm(24 h), (e) HT-rus(25 min) and (f) HT-rus(50 min).

3.3. TGA

TGA of the reconstructed samples, as well as that of the calcined sample, is shown in Fig. 8. A low weight loss was observed during the TGA experiment for the HT-cc sample (Fig. 8a), indicating that during the calcination process, practically all of the hydrotalcite was transformed into the periclase structure. All of the rehydrated solids display the two characteristic steps of weight loss of hydrotalcite-like materials in the temperature range 343–1073 K [20,21]. The first weight loss is noticed between 343 and 553 K for all samples, attributed to the loss of adsorbed and interlayer water. The second weight loss, in the temperature range 553–1073 K, is ascribed to dehydroxylation of the brucite-like sheets [13], resulting from the collapse of the meixnerite structure. In all of the reconstructed samples, the first weight loss is quite similar, suggesting the presence of similar amounts of water molecules in the interlayer space; the differences in the second weight loss are more pronounced. The degree of reconstruction of the final solids was estimated by comparing the TGA profiles with the theoretical weight loss in meixnerite-type materials; these results are summarized in Table 2. The samples prepared by mechanical stirring [HT-rm

(25 min), HT-rm(4 h) and HT-rm(24 h)] showed a low degree of reconstruction, with values of 48.0, 80.2, and 84.1%, respectively. In contrast, the sonicated samples exhibited greater reconstruction back to the meixnerite structure, suggesting the presence of a greater number of OH^- groups in the sonicated samples compared with the samples treated under mechanical stirring. This is reasonable taking into account that sonication produces materials with higher surface areas and smaller crystallites by reducing the thickness in the stacking of layers, and especially leads to the formation of irregularities in the final material. This fact derives in the presence of a larger number of exposed OH^- sites not only at the edges [23] of the meixnerite, but also at the defects of the platelets. Moreover, the sonication effect is dramatically pronounced when larger contact times are used [HT-rm(50 min) vs HT-rm(25 min)].

3.4. TPD of CO_2

The measure of the basicity of the different catalysts was obtained by TPD of CO_2. The peaks observed can be assigned based on the temperature at which they appear. Previous studies have shown that a first peak that decomposes at about 693 K can be attributed to the contribution of mainly bidentate carbonates species, together with bicarbonate species. The presence of a small peak at higher temperature (813 K) can be attributed to the presence of monodentate species [22]. Fig. 9, a and b, shows the CO_2 uptake during TPD experiments performed over two representative samples [HT-rus(50 min) and HT-rm(24 h)], prepared under mechanical stirring and ultrasound, respectively. In addition, a blank test for the HT-rm(24 h) (Fig. 9c) without the adsorption of CO_2 was performed. It is important to note that for the blank test, practically no signal of CO_2 was observed. The small traces of CO_2 observed in these samples can be attributed to the manipulation of the sample before it was introduced into the TPD equipment. This demonstrates that during the rehydration process, practically no CO_2 was adsorbed in the samples. The low-temperature peak (693 K) was detected for all of the samples regardless of the reconstruction treatment used, whereas the peak at higher temperature was seen only for the sonicated materials. The peak observed at higher temperatures can be ascribed to the presence of strong basic sites in the sonicated samples.

Integration of the profiles, calculated as the amount of CO_2 evolved on subtraction of the corresponding decomposition profile in He, is reported in Table 3. The total number of basic sites for the HT-rus(25 min) and HT-rus(50 min) samples was 1200 and 1820 μmol g_{cat}^{-1}, respectively. As determined by ICP analysis, the total number of basic sites can be calculated from the number of Al^{3+} ions present in the hydrotalcite, which is proportional to that of the compensating anions (OH^-). From the quantification in Table 3, the amount of CO_2 evolved with respect to the bulk Al content indicated that approximately 38 and 57% of the OH^- sites were detected for HT-rus(25 min) and HT-rus(50 min), respectively. In contrast, only 16 and 26% of the OH^- sites were evaluated in the HT-rm(4 h) and HT-rm (24 h) samples, respectively. This indicates that the amount of accessible Brønsted OH^- groups probed by CO_2 molecules depends on the reconstruction treatment. In particular, these re-

Table 2
Thermogravimetric analysis of hydrotalcite samples

Sample	Loss of interlayer water (wt%)[a]	Dehydroxylation (wt%)[b]	Degree of reconstruction (%)
HT-rm(25 min)	11.6	15.4	48.0
HT-rm(4 h)	14.6	25.5	80.2
HT-rm(24 h)	15.4	27.0	84.1
HT-rus(25 min)	16.4	30.0	94.0
HT-rus(50 min)	19.3	32.0	100.0

[a] 343–553 K.
[b] 553–1073 K.

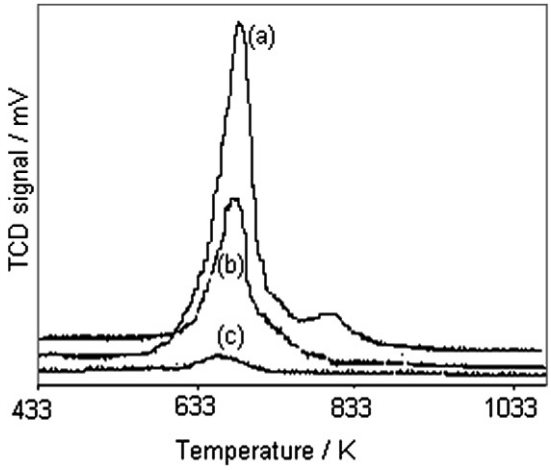

Fig. 9. CO_2 uptake during temperature-programmed desorption experiments. (a) HT-rus(50 min), (b) HT-rm(24 h) and (c) blank test of the HT-rm(24 h) without the adsorption of CO_2.

Table 3
Quantification of the basicity by CO_2-TPD profiles and benzoic acid titration for rehydrated hydrotalcites

Sample	Peak at 693 K (%)	Peak at 813 K (%)	Total CO_2 (μmol g_{cat}^{-1})	CO_2/Al ratio[a]	Benzoic acid (μmol g_{cat}^{-1})[b]
HT-rm(4 h)	100	–	520	0.16	310
HT-rm(24 h)	100	–	850	0.26	420
HT-rus(25 min)	90.5	9.5	1200 (114)[c]	0.38 (0.036)[c]	700 (120)[b]
HT-rus(50 min)	85.2	12.8	1820 (232)[c]	0.57 (0.073)[c]	1100 (190)[b]

[a] Mol of total adsorbed CO_2 per mol of Al in the HT.
[b] Mol of total benzoic acid consumed during the titration of the HT obtained from the plot of initial reaction rate versus benzoic acid amount in Fig. 11 (in parentheses, contribution from the first linear segment).
[c] In parentheses, contribution of the peak at 813 K.

sults demonstrate not only that not all of the total OH^- sites are evaluated by CO_2-TPD experiments, but also that the OH^- groups in the sonicated samples are actually more accessible. Moreover, the presence of the two peaks suggests the existence of OH^- groups with different strength. The differences in basicity of the OH^- sites in the reconstructed materials can be attributed to the existence of abundant irregularities or linear defects in the platelets of the sonicated samples, as revealed by HRTEM analysis.

Interestingly, increasing the sonication time from 25 to 50 min had little effect on the surface area of the resulting meixnerites (from 437 to 466 $m^2\,g^{-1}$). However, the number of stronger basic sites was twice as high in HT-rus(50 min). This could be explained by the greater amount of irregularities in the platelets of the latter sample, leading to a higher number of exposed OH^- sites.

3.5. Catalytic activity

The epoxidation of styrene was carried out to find structure-sensitive correlations between the rehydration methods and the presence of defects on the catalytic activity. A representative reaction profile for the epoxidation is presented in Fig. 10. In all cases, the selectivity to styrene oxide was >95%. The as-synthesized sample (HT-asy) displayed an extremely low activity (around 1.2%) of styrene conversion after 100 min of reaction. The activity of the calcined sample without water in the reaction medium, as shown in Fig. 10, was slightly higher than that obtained for the HT-asy. However, a very significant enhancement of the styrene conversion (up to 90%) was achieved after 60 min of reaction with the HT-cc sample when water was introduced in the reaction medium. The latter leads to the reconstruction of the mixed oxide during reaction [24], and further suggests that the presence of Brønsted basic sites in the catalyst is a key parameter governing the catalytic activity of this reaction.

Accordingly, the catalytic activity was significantly increased when the reconstructed materials were used in the reaction. A total styrene conversion was achieved in 60 min using the catalysts reconstructed under mechanical stirring [HT-rm(25 min) or HT-rm(4 h)], whereas the increase in catalytic activity for the samples previously treated under ultrasound [HT-rus(25 min) and HT-rus(50 min)] was more pronounced. Moreover, a catalytic activity test of the HT-rus (50 min) sample without the addition of water in the reaction medium revealed no difference in catalytic behavior. This finding indicates that for the nonrehydrated samples, the addition of water significantly improved the catalytic activity, but this was not the case for the rehydrated samples. Thus, the presence of meixnerite-like phase is the key factor to improving catalytic activity. The catalytic activity also increased with increasing surface area, from 215 $m^2\,g^{-1}$ for HT-rm(25 min up to 446 $m^2\,g^{-1}$ for HT-rus(50 min), further indicating not only that much exposed OH^- is easily accessible, and also that smaller hydrotalcite crystals (see the section on HRTEM) are present in the sonicated samples.

In the HT-rus(50 min) sample, reaching total conversion took only 30 min. From these results, it can be concluded that vigorous stirring and the use of ultrasound produce the breakup of the mixed oxides during reconstruction, leading to materials with enhanced catalytic activity. However, the initial rate of the sonicated hydrotalcite HT-rus(50 min) was ca. 6-fold higher than that of the catalyst obtained under mechanical stirring. Therefore, the formation of defects (as previously observed by HRTEM) in the sonicated samples likely accounts for the increase in the number of accessible OH^- groups.

To gain insight into the origin of the significant activity of the sonicated catalysts, and correlate it with the enhanced basicity observed during CO_2-TPD experiments, the effective base amount also was evaluated by titration with benzoic acid. To accomplish this, different amounts of benzoic acid previously dissolved in acetone were added during reconstruction of the mixed oxide by either mechanical stirring or ultrasound. The catalysts were subsequently used in the styrene epoxidation reaction; the results are presented in Fig. 11. The catalytic activity can be significantly reduced by annihilating the active sites if the latter are neutralized with benzoic acid. This implies that the addition of benzoic acid can reduce the amount of basic sites and, consequently, decrease the styrene conversion to a certain

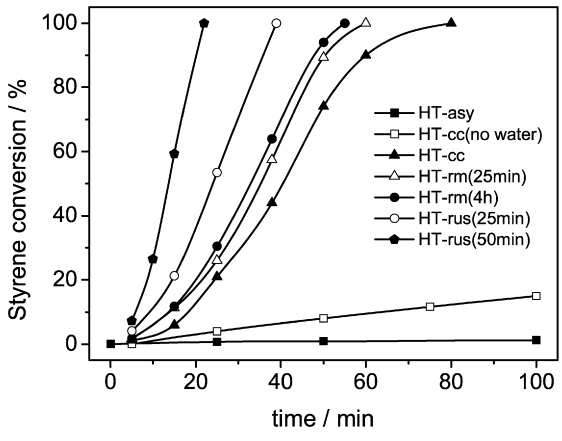

Fig. 10. Conversion vs time for the styrene epoxidation at 313 K for the different hydrotalcite samples.

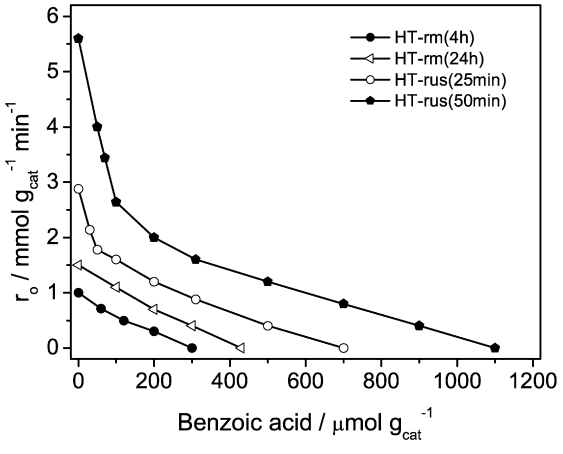

Fig. 11. Titration by benzoic acid for the determination of the base amount of the HT catalysts. Initial reaction rate versus amount of benzoic acid added.

extent. Accordingly, a linear correlation between the amount of benzoic acid and the initial rate was found for the hydrotalcites reconstructed under mechanical stirring [HT-rm(4 h) and HT-rm(24 h)]. As the amount of benzoic acid was increased, the corresponding initial reaction rate decreased until no activity was detected. Extrapolation of the linear segment at $y = 0$ leads to the amount of benzoic acid that can eliminate the catalytic activity of that catalyst. The amount of benzoic acid for these two samples was 310 and 420 μmol g_{cat}^{-1} (see Table 3), respectively. The samples treated under ultrasound exhibited different behavior on reconstruction with different amounts of benzoic acid. Fig. 11 shows two intersecting linear segments in HT-rus(25 min) and HT-rus(50 min) hydrotalcites, suggesting the existence of at least two kinetically distinguishable active OH^- sites. A very rapid decrease in the initial reaction rate (first linear segment) was observed for the HT-rus(25 min) sample, followed by a gradual decrease down to 700 μmol g_{cat}^{-1} (second linear segment).

More pronounced was the decrease in the initial reaction rate for the HT-rus(50 min) sample when small amounts of benzoic acid were added, finally reaching a total number of evaluated OH^- sites of 1100 μmol g_{cat}^{-1} until no activity could be seen. Strikingly, the existence of the two segments in the sonicated samples suggests the presence of two types of basic sites in the reconstructed hydrotalcites. This finding is in agreement with the presence of two different desorption peaks in the CO_2-TPD analysis, assigned to basic sites (OH^- groups probed by CO_2 molecules) of different strengths. In fact, the values derived from the extrapolation of the first segment to zero leads to a corresponding number of basic sites of 120 and 190 μmol g_{cat}^{-1} for HT-rus(25 min) and HT-rus(50 min), respectively, rather similar to the values obtained by CO_2-TPD (Table 3). These stronger basic sites (which are primary titrated) can be ascribed to those located at the defects (irregularities of the particles) in the sonicated samples. The results of titration experiments seem to demonstrate that not all of the basic OH^- sites in the sonicated samples are equally accessible compared with the samples treated under mechanical stirring. This implies that a relatively small amount of benzoic acid is sufficient to inhibit the catalytic performance to a significant extent, particularly in the sonicated samples; for example, adding only 190 μmol g_{cat}^{-1} of benzoic acid leads to a 2-fold decreased initial rate, with a significant number of basic sites remaining in the catalyst until final annihilation of the catalytic performance. Therefore, the catalysts prepared under ultrasound have a certain number of strong basic sites and a greater number of basic sites of medium strength. This is confirmed in the samples reconstructed under mechanical stirring, displaying lower values in the total number of basic sites. The basic sites related to the defects produced by sonication have around 6 times more activity than the basic sites obtained by disaggregation of layers. Basicity results are in good agreement with the TGA findings (Fig. 8), in which the greater weight loss of the samples reconstructed under ultrasounds leads to a higher degree of reconstruction. This derives into an increased number of accessible OH^- groups, which in fact can be detected by TPD or titration.

As demonstrated previously [9,10], proper activation of hydrotalcites is clearly a critical factor. With short sonication treatment [9], surface areas are strongly altered compared with samples treated under mechanical stirring; however, surface areas remain practically constant after longer ultrasound treatments. This indicates that sonication is not only affecting the general morphology of the samples, but also producing more irregularities or defects in the structure. This specific feature has been confirmed with HRTEM analysis (Fig. 5), leading to the conclusion that the dramatic disorder produced in the solid is responsible for the increase in the basic strength. This finding is also confirmed by our TPD experiments, which revealed an increase of the amount of CO_2 evolved in the sonicated samples compared with those reconstructed under mechanical stirring.

Indeed, it appears that the OH^- groups located at these defects are much more effective for the epoxidation reaction. The use of ultrasound for longer times leads to pronounced modifications of the particles without altering the surface area, but reinforcing the fraction of stronger ones. As supported by work by Roeffaers et al. [12], those OH^- species located in corners of the crystals likely present a stronger basicity than those located on crystal faces. In our particular case, the formation of defects favors the performance toward the epoxidation reaction.

4. Conclusion

Sonication is considered an effective way to maximize the accessibility and utility of the OH^- groups in reconstructed hydrotalcites for epoxidation reactions. This can be achieved by formation of small hydrotalcite nanoplatelets with irregularities along the platelets. The rehydration method (sonication or mechanical stirring) applied during reconstruction of the mixed oxides clearly influences the catalytic activity in styrene epoxidation. The formation of defects or distortions in the hydrotalcite nanoplatelets on longer ultrasound treatment is a powerful method for creating stronger and more active basic sites for base-catalyzed reactions

Acknowledgments

Financial support was provided by the Spanish Ministry of Education in Science (grants CTQ2006-08196/PPQ and ENE2006-06925).

References

[1] F. Cavani, F. Trifirò, A. Vaccari, Catal. Today 11 (1991) 173.
[2] S. Abelló, F. Medina, D. Tichit, J. Pérez-Ramírez, J.C. Groen, J.E. Sueiras, P. Salagre, Y. Cesteros, Chem. Eur. J. 11 (2005) 728.
[3] D. Tichit, B. Coq, CATTECH 7 (2003) 206.
[4] F. Figueras, J. Lopez, J. Sánchez-Valente, T.T.H. Vu, J.M. Clacens, J. Palomeque, J. Catal. 211 (2002) 144.
[5] Y. Ono, J. Catal. 216 (2003) 406.
[6] M.L. Kantam, B.M. Choudary, C.V. Reddy, K.K. Rao, F. Figueras, Chem. Commun. 9 (1998) 1033.
[7] M. Adachi-Pagano, C. Forano, J.-P. Besse, Chem. Commun. (2000) 91.
[8] J.C.A.A. Roelofs, A.J. van Dillen, K.P. de Jong, Catal. Today 60 (2000) 297.

[9] S. Abelló, F. Medina, D. Tichit, J. Pérez-Ramírez, Y. Cesteros, P. Salagre, J.E. Sueiras, Chem. Commun. (2005) 1453.
[10] F. Winter, X. Xia, B.P.C. Hereijgers, J.H. Bitter, A.J. van Dillen, M. Muhler, K.P. de Jong, J. Phys. Chem. B 110 (2006) 9211.
[11] F. Winter, A.J. van Dillen, K.P. de Jong, Chem. Commun. (2005) 3977.
[12] M.B.J. Roeffaers, B.F. Sels, H. Uji-i, F.C. De Schryver, P.A. Jacobs, D.E. De Vos, J. Hofkens, Nature 439 (2006) 572.
[13] F. Cavani, F. Trifirò, A. Vaccari, Catal. Today 11 (1991) 173.
[14] K. Rao, M. Gravelle, J. Valente, F. Figueras, J. Catal. 173 (1998) 115.
[15] A.J. Jacobson, Mater. Sci. Forum 152–153 (1994) 1.
[16] N. Miyamoto, H. Yamamoto, R. Kaito, K. Kuroda, Chem. Commun. (2002) 2378.
[17] A. Takagi, M. Sugisawa, D. Lu, J.N. Kondo, M. Hara, K. Domen, S. Hayashi, J. Am. Chem. Soc. 125 (2003) 5479.
[18] R. Ma, Z. Liu, L. Li, N. Iyi, T. Sasaki, J. Mater. Chem. 16 (2006) 3809.
[19] L. Li, R. Ma, Y. Ebina, Y.N. Iyi, T. Sasaki, Chem. Mater. 17 (2005) 4386.
[20] E. Kanezaki, Inorg. Chem. 73 (1998) 2588.
[21] W.T. Reichle, J. Catal. 94 (1985) 547.
[22] V.K. Díez, C.R. Apesteguía, J.I. Di Cosimo, J. Catal. 215 (2003) 220.
[23] J.C.A.A. Roelofs, A.J. van Dillen, K.P. de Jong, Catal. Today 60 (2000) 297.
[24] I. Kirm, F. Medina, X. Rodríguez, Y. Cesteros, P. Salagre, J. Sueiras, Appl. Catal. A Gen. 272 (2004) 175.